Graphene Supported Silver Nanocrystals Preparation for Efficient Oxygen Reduction in Alkaline Fuel Cells

Mohammad Shamsuddin Ahmed, Dong-Weon Lee, and Young-Bae Kim[z]

Department of Mechanical Engineering, Chonnam National University, Gwangju, South Korea

The silver nanocrystals (AgNCs) anchored on graphene oxide (GO) catalysts have been synthesized by a facile chemical reduction and nontemplate method using ascorbic acid (AA) as reducing agent and have successfully employed as a cathode catalyst for oxygen reduction reaction (ORR) in direct alkaline fuel cells (DAFCs). The morphological characterizations demonstrate that the AgNCs have crystalline form and grafted onto reduced graphene oxide (AgNCs/rGO_AA). Comparatively better dispersion and higher population of AgNCs have observed on AA treated AgNCs/rGO than $NaBH_4$ which is known as conventional reducing agent. The electrochemical catalysis in 0.1 M KOH electrolyte has demonstrated that the AgNCs/rGO_AA has an excellent electrocatalytic activity for ORR in alkaline media compared to the other tested electrodes. Particularly, it shows 40% higher mass activity with large specific activity against 20 wt% Pt/C with faster electron transfer rate per O_2. Moreover, the reaction kinetic parameters have confirmed that the ORR at AgNCs/rGO_AA catalyst not only follows a $4e^-$ process with lowering H_2O_2 formation but also proceeds on with good stability and fuel selectivity in DAFCs.

Manuscript submitted May 19, 2016; revised manuscript received August 1, 2016. Published August 12, 2016.

The oxygen reduction reaction (ORR) is an interesting research area and already attracted widespread attention of researches from all over the world because of its important role in the application of energy storage and conversion devices, such as fuel cells (FCs) and metal−air batteries in alkaline media.[1–4] Due to superior energy conversion efficiency and potential for providing clean energy, FCs are in the main attention as next generation energy sources.[5,6] As the FCs consists of anode and cathode electrodes, the greatest effect on the performance of FCs is the oxidation/reduction reaction kinetics occurring at the respective electrodes. Unfortunately, the sluggish kinetic rate of ORR at the cathode is the main obligation to be applied in industry.[6]

Typically, the platinum (Pt) and/or Pt-based materials are known as the most efficient electrocatalyst in the cathode for ORR catalysis[7–10] but unfortunately, the Pt-based materials have faced many troubles such as its susceptibility to time dependent drift and CO poisoning,[11,12] slow electron-transfer kinetics,[13] high costs, limited supply,[14] and poor durability.[15] For those reasons, Pt has hindered the widespread commercialization of FCs technology. To overcome the cost challenges, significant efforts have focused on the development of alternative non-Pt catalysts that are based on mainly non-precious metals and/or various heteroatom-doped carbonaceous materials.[16–18] Among the non-Pt metal catalysts studied, silver (Ag)-based carbon nanomaterials have been explored as promising candidates with higher activity and stability in alkaline medium recently.[19–22] According to previous reports, the Ag is an ideal alternative of Pt because it is not only abundantly available in nature and much cheaper but also higher electrical and thermal conductive than Pt.[23,24] Previous research also revealed that the Ag-based catalysts have higher catalytic activity for ORR[25] and superior stability in alkaline media.[26]

The graphene oxide (GO)[27] is the oxidized and exfoliated sheet of graphene which distorted sp^2 carbon networks carrying mainly epoxide (−O−), hydroxyl (−OH), carbonyl (−C=O), and carboxyl (−COOH) groups. The large scale preparation of high-quality graphene is easily possible by chemical reduction of GO[18,28–30] rather than other methods.[31–34] For the preparation of reduced graphene oxide (rGO) via chemical reduction, however, reducing agents such as, hydrazine (N_2H_4),[35,36] N,N-dimethylhydrazine,[37] hydroquinone[38] and sodium borohydride ($NaBH_4$)[39] have been used. Unfortunately, because of their toxic and explosive properties, safety precautions must be taken when large quantities of these reagents are used.[18,34] Also, some reductants like N_2H_4 or thermal treatment (in presence of other foreign molecules) are often introduces heteroatoms into the graphene plane to produce doped graphene[40,41] that could show certain ORR activities with losing the purity of graphene.[42] Moreover, particular reducing agent has the specific oxygenated group removal efficiency. For example, the Nagase group[43] has found that the N_2H_4 and thermal treatment could efficiently remove the epoxide group (plane) than −COOH (edge) from GO. They also observed that the −COOH group is comparatively difficult to remove than other oxygenated groups.[43,44] As many previous reports have reported an interesting fact, however, the list amount of −COOH group containing rGO showed better ORR activity,[18,45–47] because it improves the edge of rGO which facile to the charge polarization of edge carbon atoms.[4] In this regards, the high-quality and high-purity rGO production by L-ascorbic acid (AA) can be the harmless and easy approaches with much reduction of −COOH group from GO edge[48,49] and this is first time we have applied AA reduced AgNCs anchored rGO (AgNCs/rGO) for ORR catalysis.

In this study, we have prepared AgNCs/rGO via simple chemical reduction process with AA (denoted as AgNCs/rGO_AA) for better ORR catalysis which has the following merits: First, the AgNCs/rGO_AA catalyst is easily synthesized, and the AgNCs have monolayer dispersion with comparatively higher population onto the graphene. Second, the –COOH group has removed significantly from rGO by AA-reduction treatment which facile to the ORR kinetics by improving sp^2 carbon network at the edge of graphene plane. Third, Ag can be found as crystalline form while oxide form may have adverse effect.[50] Fourth, the as-prepared AgNCs/rGO_AA exhibits higher electrocatalysis toward ORR even than that of state-of-the-art Pt/C with long term stability.

Experimental

Synthesis of AgNCs/rGO_AA.—GO was prepared from graphite powder via a modified Hummer's method.[11,51] 10 mg GO was loaded into a 50-mL flat bottom vial, followed by the addition of 15 mL of water. A yellow-brown homogeneous solution was prepared by ultrasonic agitation until it became clear with no visible large particulate. Then, 10 mL of 10 mM $AgNO_3$ water solution was added into the above solution and kept under stirring for overnight. Subsequently, 2 mL of 0.1 M AA solution was added into the above mentioned solution and stirring was continued for a day. A homogeneous black suspension was then produced after heating in an oven at 65°C for overnight. Finally, the obtained material, AgNCs/rGO_AA, was filtered, washed two times with water and dried at 60°C for another 12h. For comparison, the rGO_AA and AgNCs/rGO_$NaBH_4$ were prepared without addition of $AgNO_3$ and with the addition of 0.1 M $NaBH_4$ instead of 0.1 M AA, respectively.

[z]E-mail: ybkim@chonnam.ac.kr

Physical characterization of AgNCs/rGO_AA.—Transmission electron microscopy (TEM) images and energy-dispersive X-ray spectroscopy (EDX) were obtained by TECNAI model FI-20 (FEI, Netherland). Raman spectra were obtained with LabRam HR800 UV Raman microscope (Horiba Jobin-Yvon, France), with an excitation of 514 nm Ar^+ laser. X-ray photoelectron spectroscopic (XPS) were gained using a MultiLab 2000 with a 14.9 keV Al K X-ray source and curve fitting was done with an XPSPEAK41 system software. X-ray diffraction (XRD) spectra were carried out on a Rigaku D/max-2500, using filtered Cu Kα radiation.

Electrochemical characterization.—The 1 mg mL^{-1} suspension of AgNCs/rGO_AA was prepared in water by ultrasonication. A 10 μL portion of AgNCs/rGO_AA ink was then dropped onto the pre-polished glassy carbon electrode (GCE, 0.0707 cm^2) Ag loading was 24.76 μg cm^{-2}. The rGO_AA and AgNCs/rGO_$NaBH_4$ (Ag loading 27.73 μg cm^{-2}) coated GCEs were prepared follower by the same protocol. The commercially available Pt/C suspension (Johnson Matthey 20 wt% on Vulcan XC-72) was prepared by dispersing 1 mg mL^{-1} of Pt/C in ethanol in the presence of 5 μL of 5% Nafion solution (in alcohol) and used 10 μL from the suspension onto GCE (Pt loading was 28.3 μg cm^{-2}). All electrochemical measurements including cyclic voltammetry (CV) and chronoamperometry (CA) were taken using a three-electrode potentiostat [CHI 700C electrochemical workstation (U.S.A.)]. A Pt wire and Ag/AgCl electrodes were used as auxiliary electrode and reference electrode, respectively. The potential of the Ag/AgCl reference electrode was corrected with the reversible hydrogen electrode (RHE), $E_{(RHE)} = E_{(Ag/AgCl)} + 0.982$ V. All electrochemical experiments were performed in a high purity argon (Ar)- and/or O_2-saturated 0.1 M KOH (pH 13) solutions at room temperature (RT, ~25°C).

Calculations.—The electrochemical surface area (ECSA) calculation

$$\text{ECSA} = \frac{Q_0}{Q_r \times m} \quad [1]$$

where, Q_o is the charge for oxide-reduction peak during a cathodic scan (in μC cm^{-2}), m is the metal loading (in μg cm^{-2}) over the GC working electrode, and Q_r is the charge required for the monolayer adsorption of oxygen on Ag surface (420 μC cm^{-2})[4] or the charge required for monolayer adsorption of hydrogen on Pt surface (210 μC cm^{-2}).[52]

n-calculation by CVs data:[53]

$$i_p = 0.4958nFAC_{O_2}\left(\frac{\alpha n_\alpha F}{RT}\right)^{0.5} v^{0.5} D_{O_2}^{0.5} \quad [2]$$

$$\Delta E_p = \frac{1.15\,RT}{\alpha n_\alpha F} \quad [3]$$

where, i_p is the peak current, n is the number of transferred electrons, A is the surface area of the GCE (0.0707 cm^2), F and T are Faraday constant (96485.3 C mol^{-1}) and the temperature, D_{O_2} and C_{O_2} are the oxygen diffusion coefficient (1.9 × 10^{-5} cm^2 s^{-1}) and the bulk concentration (1.2 mmol L^{-1}), respectively; v is the scan rate in V s^{-1}, α is the transfer coefficient, n_α is the apparent number of electrons transferred in the rate-determining step and ΔE_p is the peak potential change when the scan rate increases 10-fold.

n-calculation by Koutecky-Levich equation[6,17]

$$\frac{1}{J} = \frac{1}{J_k} + \frac{1}{J_L} \quad [4]$$

$$J_L = 0.62nFAD_{O_2}^{2/3} C_{O_2} v^{-1/6} \omega^{1/2} \quad [5]$$

herein, J, J_k, and J_L are the measured, kinetic, and diffusion limiting current densities (mA cm^{-2}), respectively, v is the kinetic viscosity of the electrolyte (1 × 10^{-2} cm^2 s^{-1}), ω is the rotation rate of electrode (rpm).

n and % of H_2O_2-calculation by rotating ring-disk electrode (RRDE)[6,17]

$$n = \frac{4i_d}{i_d + \left(\frac{i_r}{N}\right)} \quad [6]$$

$$H_2O_2\,\% = \frac{200i_d}{i_d + \frac{i_r}{N}} \quad [7]$$

$$N = \frac{-i_r}{i_d} \quad [8]$$

where, N is the collection efficiency of RRDE (0.37), and i_d and i_r are the disk and ring electrode currents, respectively.

Current density calculation[4]

$$J_k = \frac{J_L \times J}{J_L - J} \quad [9]$$

Result and Discussion

Instrumental characterization.—The TEM images of AgNCs/rGO_AA and AgNCs/rGO_$NaBH_4$ catalysts are shown in Figure 1 and all are consisting of AgNCs onto the graphene plane. Accordingly, various sizes of AgNCs are coexisting onto the rGO sheet; most of the AgNCs are nano-sized and spherical in shape. Figure 1a shows an irregular size and higher aggregation with lower population of AgNCs onto rGO sheet at AgNCs/rGO_$NaBH_4$ sample. On the other hand, Figure 1b shows monodispersed with higher population and nano-sized AgNCs anchored onto the surfaces of rGO sheet with the average size of 8.8 nm at AgNCs/rGO_AA sample. The high-resolution TEM (HRTEM) images (Figure c) show an AgNC of AgNCs/rGO_$NaBH_4$ (i) and AgNCs/rGO_AA (ii) lattice lines are visible clearly. Only one (111) plane can be visible (d-spacing of 0.235 nm) from AgNC of AgNCs/rGO_$NaBH_4$. Whereas the AgNC of AgNCs/rGO_AA which maintained a highly ordered crystalline structure and most of the population consisted of single crystalline AgNCs with multi lattice d-spacing of 0.202, 0.235 and 0.295 nm, which corresponds to the (200), (111) and (110) planes of AgNC, respectively.[54,55] Also comparing with more HRTEM images (Figure S1), at AgNC of AgNCs/rGO_AA, the measured fringe spacing are 0.25 nm and 0.15 nm, which correspond well with the spacing between 1/3(422) and (220) planes of the face centered cubic (FCC) AgNC, respectively.[55] The corresponding EDX spectra with the numerical analysis of elements in all AgNCs/rGO samples have also observed (Figure S2). In the case of the AgNCs/rGO hybridized nanostructures, C, O and Ag elements could be detected distinctly. Also, besides those elements, Cu element could also be detected due to Cu TEM grid. To determine the surface area, we measured the Brunauer–Emmett–Teller (BET) surface area of pure both catalysts using liquid nitrogen adsorption–desorption isotherms (Figure 1d). Figure 1d shows the isotherm curves of AgNCs/rGO_$NaBH_4$ (i) and AgNCs/rGO_AA (ii). The specific surface area of both samples is shown in the figure. The AgNCs/rGO_AA catalyst was found to exhibit the largest surface area, 49.6 m^2 g^{-1}, than AgNCs/rGO_$NaBH_4$ (36.6 m^2 g^{-1}).

The crystalline structure of the obtained materials was studied by XRD technique. As shown in Figure 2a, the diffraction peaks appearing at ~25.5° in XRD patterns of all samples can be ascribed to the (002) plane of graphitic carbon (ICSD Ref. 98-005-2230), suggesting, the GO has been reduced to rGO upon reduction treatment.[56] It is, however, the prominent peaks at 38.1°, 44.2°, 64.3° and 77.3° were assigned to the (111), (200), (220) and (311) crystallographic planes of the FCC AgNCs, respectively [ICSD Ref. 98-005-3759].[57] An interesting observation has found in Figure 2a inset. Primarily, XRD patterns of all samples are negatively shifted compared to the AgNCs reference due to the attachment of rGO. Moreover, the XRD pattern of $NaBH_4$ treated AgNCs/rGO is shifted more toward lower 2θ value as compared to the AA treated AgNCs/rGO. This implies that the AgNCs upon $NaBH_4$ treatment have slightly higher lattice

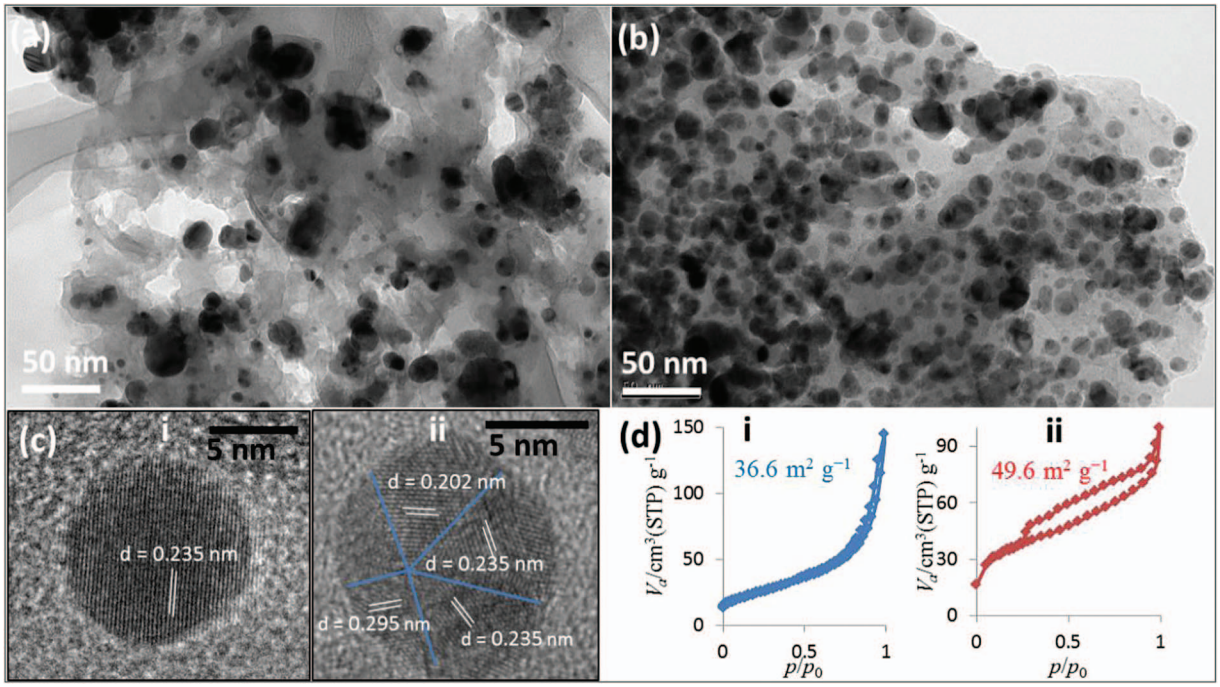

Figure 1. The TEM images (a and b), the corresponding HRTEM images (c) and the BET surface area calculated from nitrogen adsorption–desorption isotherms (d) of AgNCs/rGO_NaBH$_4$ (a, c-i, d-i), AgNCs/rGO_AA (b, c-ii, d-ii).

parameter as compared to the AgNCs upon AA treatment. Such kind of anomalies has attributed to the prevalence of point defects such as oxide formation.[11,58] The average nanocrystal size of each catalyst was calculated from Ag(111) peak using Scherrer formula.[11] The sizes were estimated as 8.8, and 8.1, nm for AgNCs/rGO_AA, and AgNCs/rGO_NaBH$_4$, respectively, which are in good agreement with the predetermined particle sizes by HRTEM.

Raman spectroscopy has used to figure out the degree of GO reduction upon addition of reducing agents in the as prepared catalysts (Figure 2b). Typically, Raman spectra have two major bands, the D band (at ~1350 cm^{-1}) is a breathing mode of k-point phonons of A_{1g} symmetry and G band (at ~1600 cm^{-1}) is assigned to the E_{2g} phonon of C sp^2 atoms. Prominent D band in the Raman spectrum is an indication of disorder of graphene sheets, which originating from defects associated.[2,18] The intensity ratio of the D band to the G band (I_D/I_G) of the rGO_AA, AgNCs/rGO_AA, and AgNCs/rGO_NaBH$_4$ were calculated as 0.93, 0.93 and 0.95, respectively, which indicating an improved sp^2 domain of the carbon network at rGO_AA and AgNCs/rGO_AA upon AA treatment than that of NaBH$_4$ treatment.[59] In addition, The G band of the AgNCs/rGO samples was shifted to higher wavelength (Figure S3) compared to rGO, which suggests the conjugated network was introduced by other component like AgNCs.[60] Importantly, such a shift in rGO-based hybrids may result from charge transfer between carbon network and AgNCs[61] as the higher G band shift found at AgNCs/rGO_AA than AgNCs/rGO_NaBH$_4$. Therefore, the result confirms the higher degree of GO reduction with sp^2 conjugated network restoration and the higher charge transfer between rGO and AgNCs at AA treated samples than NaBH$_4$ treated sample.

Two major questions are still unsolved, first, what the exact configuration of oxygenated groups reduction upon reductant addition in as prepared rGO, and second, the confirmation of metallic nature of the AgNCs which are intimately related to the electrocatalytic performance of catalysts. To resolve those questions, the as prepared samples were further investigated using XPS in Figure 3. The XPS survey spectrum of GO and rGO_AA show the presence of only C (~285.5 eV) and O (~533.5 eV) elements. On the other hand, all other AgNCs/rGO samples show various visible peaks corresponding to Ag along with the C and O elements (Figure 3a).[20,21] The C/O ratio was determined as 1.69, 4.36, 4.33 and 3.83 for GO, rGO_AA, AgNCs/rGO_AA and AgNCs/rGO_NaBH$_4$ samples,

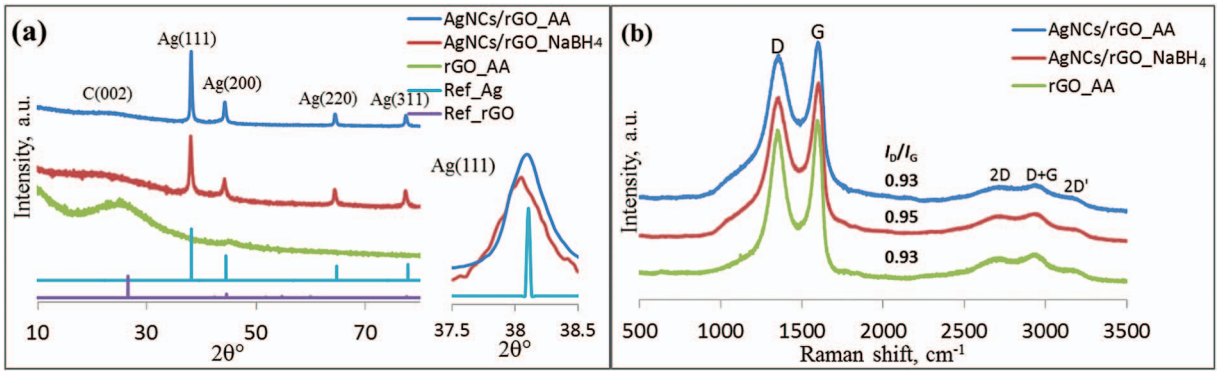

Figure 2. XRD spectrum (a) and Raman spectrum (b) of rGO_AA, AgNCs/rGO_NaBH$_4$, and AgNCs/rGO_AA; insets: the enlarged XRD spectrum at Ag(111) region, and the intensity ration of D and G band.

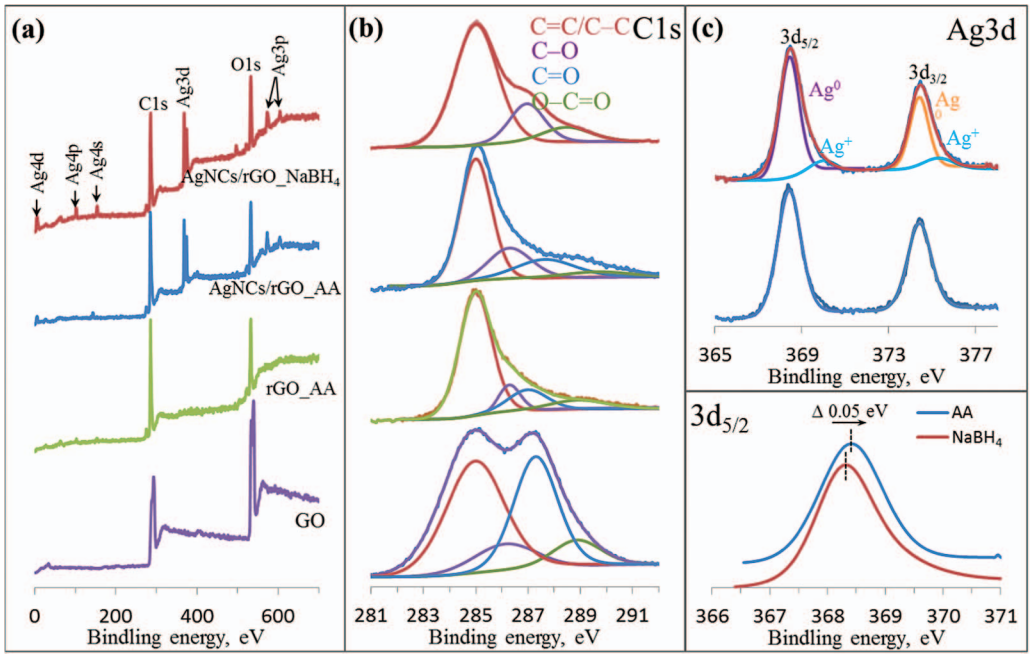

Figure 3. XPS survey spectrum (a) core level of C1s (b), O1s (d) and Ag3d (d) spectrum of rGO_AA, AgNCs/rGO_NaBH$_4$, and AgNCs/rGO_AA; XPS spectrum of GO has shown for comparison.

respectively, which signifying the reduction GO upon reduction treatment. The high-resolution C1s spectra of GO in Figure 3b shows four absorbance peaks of oxygen-free carbon (C–C and/or C=C) at 285.1 eV, C–O carbon at 286.4 eV, C=O carbon at 287.4 eV, and O–C=O carbon at 288.7 eV, respectively. This result indicates that the GO contains abundant oxygen-containing groups.[27,61,62] All samples show a strong suppression for the oxygen-containing components of their C1s XPS spectra than GO. Indicating a significant reduction of oxygenated functional groups.[2,18] An important comparison can be made in all oxygen-containing components; all oxygenated-C have reduced tremendously upon AA treatment even than that of conventionally used reductant, NaBH$_4$ (Figure S4). Very particularly, O–C=O has reduced up to 2% or 3% (for AgNCs/rGO_AA or rGO_AA) from 12.6% (for GO) while 6.5% was reduced upon NaBH$_4$ treatment which indicating the AA treated rGO edge is much improved than that of NaBH$_4$ treated rGO edge. Also, oxygenated-C peaks are little shifted compared to GO and/or rGO_AA which indicating an interaction between AgNCs and rGO through chemisorption.[11] Therefore, a significant reduction of oxygenated functional groups and better sp^2 conjugated network restoration was observed in AgNCs/rGO_AA than all other samples which was confirmed earlier by Raman analysis. The core level of Ag3d spectrum of all AgNCs containing catalysts show two major peaks for the 3d$_{5/2}$ and 3d$_{3/2}$ components at 368.4 and 374.4 eV, respectively (Figure 3c), and no any additional peak for AgNCs/rGO_AA. It is, however, other weak peaks at 370.4 and 376.1 eV can be assigned to Ag$^+$ ion at AgNCs/rGO_NaBH$_4$.[63] It indicates that Ag$^+$ ion has been completely reduced upon chemical reduction by AA and AgNCs are mainly in the metallic form (Ag^0). The calculative values of Ag$^+$ ion existence are 13.1% and 0.4% upon NaBH$_4$ and AA treatment, respectively, which is coincided with the XRD result. Also, the positive shift of Ag3d$_{5/2}$ peak has been observed. Such positively shifted value signifies oxide formation at AgNCs/rGO_NaBH$_4$ sample. The Ag content was estimated as 2.45 at% and 2.82 at% for AgNCs/rGO_AA and AgNCs/rGO_NaBH$_4$, respectively.

The electrocatalytic ORR.—To investigate the electrocatalytic activities of as prepared catalysts, the CVs in Ar and O$_2$-saturated 0.1 M KOH solutions at different modified GCEs were measured at a constant active mass loading and all the electrodes showed a substantial ORR process in the presence of oxygen (Figure 4). In Figure 4a, a single cathodic onset potential (E_{onset}) at 0.72 V (vs. RHE) can be observed in an O$_2$-saturated solution for the rGO_AA electrode and have the similar ORR E_{onset} (0.78 V vs. RHE) with little higher current for the AgNCs/rGO_NaBH$_4$ electrode. Compared with those electrodes, AgNCs/rGO_AA shows a greatly positive shift in the ORR E_{onset} (0.91 V vs. RHE) with a more pronounced increase in the cathodic current. The comparison of ORR peak current intensity can be observed in the Figure 4a inset. Moreover, the CVs of the AgNCs/rGO_AA show a larger background current than other tested samples. It may be attributed to the increase of the edge plane site (which is already proven by nitrogen adsorption–desorption isotherm experiment) due to better removal of −COOH group from GO edge, resulting in improving the capacitance current.[62] These results clearly demonstrated a significant enhancement in the ORR electrocatalytic activity for the AgNCs/rGO_AA in respect to the other tested electrodes. The number of transferred electron (n) can be primarily calculated by Equation 2[53] using the ORR peak potential changes by10-fold of scan rate increases (Figure S5). The calculated values are 3.96, 3.55, and 3.22 for AgNCs/rGO_AA, AgNCs/rGO_NaBH$_4$ and rGO_AA, respectively.

The ECSA for all AgNCs/rGO and Pt/C catalysts was calculated (Equation 1) using Coulombic charge (Q) for the AgO reduction peak[4] and hydrogen adsorption at Pt region,[8] respectively (colored peaks in Figure S6). The values of the ECSAs are summarized in Table I. The highest value was obtained for AgNCs/rGO_AA (80 m^2 g_{Ag}^{-1}) among all catalysts which is ∼1.1 and ∼2 times higher compared to Pt/C (71.9 m^2 g_{Pt}^{-1}) and AgNCs/rGO_NaBH$_4$ (41.7 m^2 g_{Ag}^{-1}), respectively. This result implies a better utilization of Ag with comparatively smaller amount on the surface of the AgNCs/rGO_AA.

To gain further insight into the ORR with these samples, linear sweep voltammetry (LSV) measurements were performed on a rotating-disk electrode (RDE) for all as prepared samples and Pt/C electrocatalyst in O$_2$-saturated 0.1 M KOH at a constant rotation speed of 1600 rpm in Figure 4b. As can be seen, the ORR at the rGO_AA and AgNCs/rGO_NaBH$_4$ electrodes has commenced around 0.72 V and 0.78 (vs. RHE), whereas the ORR E_{onset} at the AgNCs/rGO_AA electrode significantly shifted positively to 0.91 V (vs. RHE) with the higher limiting current density (J_L, mA cm^{-2}) which is the similar result observed by CVs earlier. The ORR half wave potential ($E_{1/2}$) for ORR at AgNCs/rGO_AA is only 15 mV lower and the J_L is higher (∼20% at −0.1 V vs. RHE) than that of Pt/C. These experimental

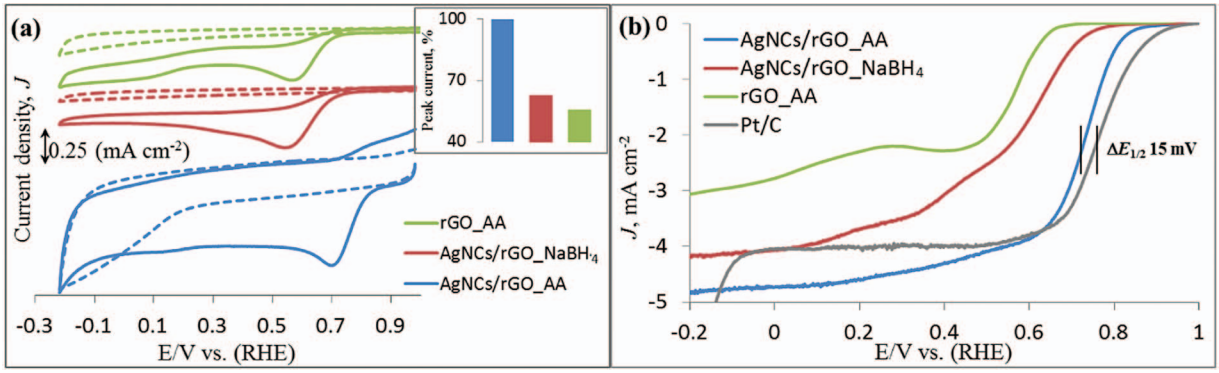

Figure 4. CV curves on all prepared catalysts in Ar (dashed lines) and O_2-saturated (solid curves) 0.1 M KOH solution at a scan rate of 50 mV s^{-1} (a), LSV curves for ORR on rGO_AA, AgNCs/rGO_$NaBH_4$, AgNCs/rGO_AA and Pt/C catalysts in O_2-saturated 0.1 M KOH solution at a scan rate of 10 mV s^{-1} and 1600 rpm (b); insets: the ORR peak current intensity as %.

results suggest that the catalytic activity of ORR at AgNCs/rGO_AA is obviously better than that of commercial Pt/C and other tested catalysts. However, it is undoubted that the well-dispersion of highly crystalline AgNCs and better reduction degree with improved edge of rGO play the key role for ORR activity enhancement of this catalyst.

The kinetics of ORR.—RDE voltammetry measurements at various rotation speeds were also carried out to gain further insight into the ORR performance of all the AgNCs/rGO electrodes in Figure 5. Figure 5 shows the RDE voltammograms of AgNCs/rGO_AA (a), and AgNCs/rGO_$NaBH_4$ (b) at scan rate of 10 mV s^{-1}. There are some important facets that warrant attention here. First, cathodic currents became clearly recognized as the electrode potential was swept in the negative direction, and the currents increased with increasing rotation speeds, signifying the apparent electrocatalytic activity of ORR at all catalysts. Second, the ORR J_L and E_{onset} at the AgNCs/rGO_AA were always larger than that of the AgNCs/rGO_$NaBH_4$ electrode at any constant rotation speed. Third, the J_L is nearly constant/linear for long range potentials (from ~0.6 to −0.2 V vs. RHE) at AgNCs/rGO_AA, while J_L lost their linearity within this potential range at AgNCs/rGO_$NaBH_4$ electrode, signifying the fast electron transfer rate at AgNCs/rGO_AA electrode. As a whole, this result indicating better ORR kinetics could be possible at AgNCs/rGO_AA rather than the AgNCs/rGO_$NaBH_4$. Also, the better linear relationship of Koutecky-Levich (K-L) plots was observed for AgNCs/rGO_AA electrode at various potentials than that of the AgNCs/rGO_$NaBH_4$ modified electrodes (Figure 5a′, and 5B′) which suggesting the slope of those plots and corresponding n values could be similar for ORR and represents first order kinetics with respect to O_2.[64] Therefore, the n values per O_2 involved in the ORR at both AgNCs/rGO electrodes were calculated again by the K-L Equation 4[17,62,64] which are similar to the calculation by CVs earlier (Figure 5 insets). Indicating the ORR proceeds via a four-electron ($4e^-$) pathway at AgNCs/rGO_AA than AgNCs/rGO_$NaBH_4$ electrode.

To further verify the ORR catalytic pathways on all AgNCs/rGO catalysts including Pt/C, we also conducted the RRDE measurements at 10 mV s^{-1} with a constant rotation speed of 1600 rpm and Pt-ring was set at constant potential of 1.2 V (vs. RHE) in Figure 6a. Figure 6a shows the disk (down) and ring (up) currents for all the electrodes. The ring currents are indicating the production of the amount of generated H_2O_2.[2,29] As can be seen, all of the modified electrodes started to generate the ring current at the ORR E_{onset}. However, the amount of H_2O_2 generated on the AgNCs/rGO_AA electrode is significantly lower than that on the AgNCs/rGO_$NaBH_4$ electrodes and similar to the Pt/C, indicating that AgNCs/rGO_AA is an efficient ORR electrocatalyst. The n values and H_2O_2 formation yields were further calculated from the given Equations 6 and 7[6,17,65,52] based on the RRDE data. As shown in Figure 6b, the n value increases with a decreasing of the negative potential. The n value for ORR at the AgNCs/rGO_AA electrode is always higher than that on the AgNCs/rGO_$NaBH_4$ modifier electrode and even better to the Pt/C over the potential range covered in this study. These are consistent with the results obtained from the K–L plots based on the RDE measurements, further suggesting the ORR catalyzed by AgNCs/rGO_AA catalyst is mainly by a $4e^-$ process. The corresponding measured H_2O_2 yields for the AgNCs/rGO_AA and Pt/C samples are 6.6~4.4%, and 8.8~9.4%, respectively, over the examined potential range. The lower n value and higher H_2O_2 formation are observed at AgNCs/rGO_$NaBH_4$ sample, which signifying a poor ORR catalysis at AgNCs/rGO_$NaBH_4$ sample. It is clear that the calculated K–L plots and n values are demonstrating a dominant $4e^-$ involved ORR process on the AgNCs/rGO_AA catalyst than AgNCs/rGO_$NaBH_4$, even better to ORR catalyzed by the

Table I. Electrocatalytic properties toward ORR of all tested metallic catalysts.

		20 wt% Pt/C	AgNCs/rGO_AA	AgNCs/rGO_$NaBH_4$
Metal loading (μg cm^{-2})		28.3	24.76	27.73
ECSA (m^2 g_M^{-1})		71.9	80	41.7
ORR E_{onset} (V vs. RHE)		0.95	0.91	0.81
J_k (mA cm^{-2})	@ 0.7 V	9.0	9.4	1.8
	@ 0.0 V	11.1	15.6	10.2
MA (mA g_M^{-1})	@ 0.7 V	0.316	0.38	0.063
	@ 0.0 V	0.39	0.55	0.33
SA (mA cm^{-2})	@ 0.7 V	0.12	0.12	0.05
	@ 0.0 V	0.15	0.2	0.14
e^- number @ −0.1 V		3.97	4.0	3.6
H_2O_2 (%) @ −0.1 V		8.9	4.6	17.5
Tafel slope (mV dec^{-1})		121	118	151
Stability by CA (J_f/J_i) %		16.2	63.5	34.3

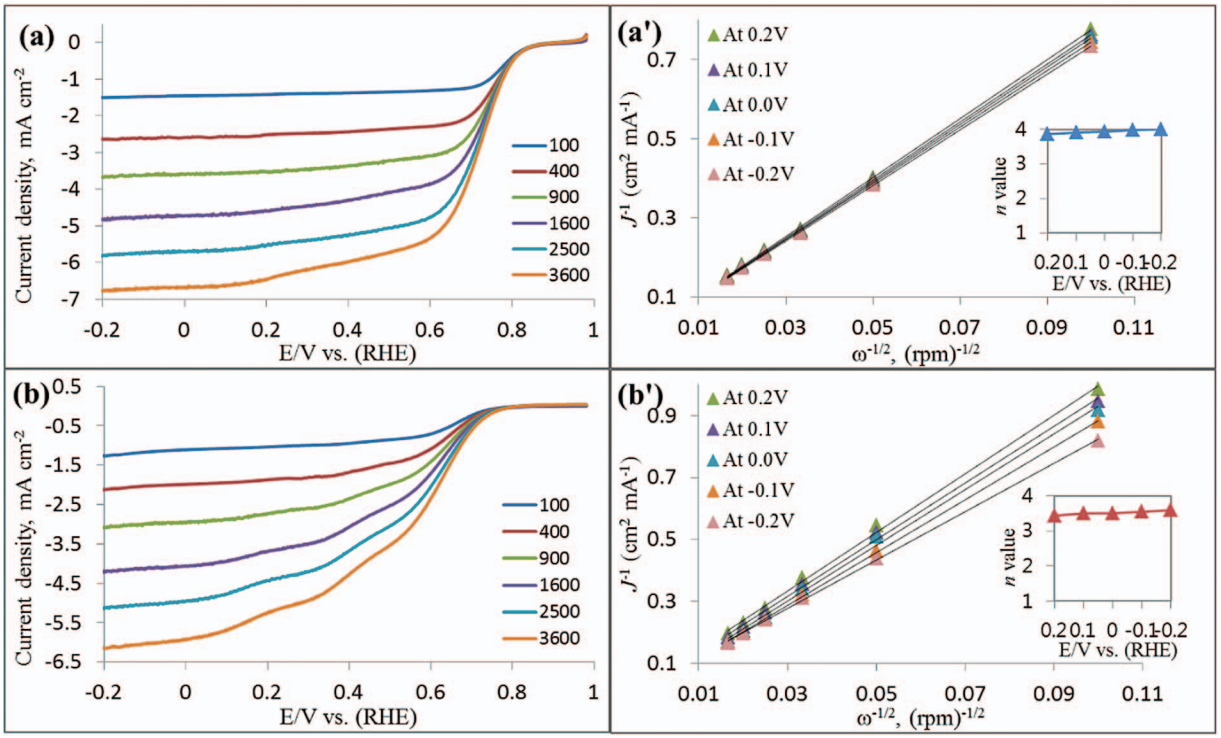

Figure 5. LSV curves at various rotation speeds for ORR at AgNCs/rGO_AA (a) and AgNCs/rGO_NaBH$_4$ (b) in an O_2-saturated 0.1 M KOH solution at a scan rate of 10 mV s^{-1}; and their corresponding K-L plot; inset: the dependence of the transferred electron number by K-L equation.

commercial Pt/C catalyst in respect to the *n* value and H_2O_2 formation. All metallic catalysts were also evaluated in terms of specific activity (SA) and mass activity (MA) (Figures 6c and 6d). The SA and MA are given as kinetic current densities (J_k) at 0.7 V (Figure 6c) and at 0.0 V (Figure 6d) normalized in reference to the loading amount of metal and ECSA, respectively,[52,66] (Table I). Of particular interest was the large SA (at 0.0 V) of AgNCs/rGO_AA, 0.2 mA cm^{-2}, exceeding the Pt/C (0.15 mA cm^{-2}) by a factor of 1.3; whereas SA

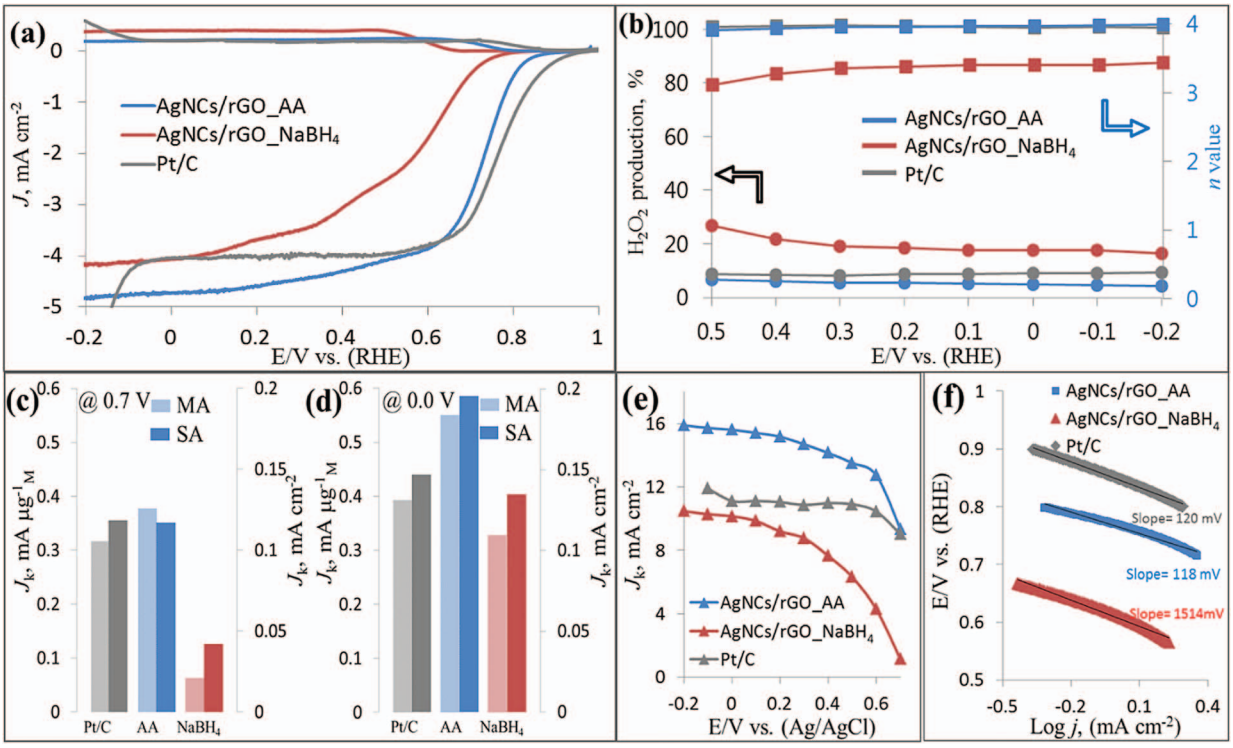

Figure 6. RRDE curves for ORR in an O_2-saturated 0.1 M KOH solution at a scan rate of 10 mV s^{-1} at 1600 rpm (a), the dependence of the electron transfer number and corresponding H_2O_2 formation (b); the comparison of MA and SA at 0.7 V (c) and 0.0 V (d); the current density (e) and the Tafel plot (f) of AgNCs/rGO_AA, AgNCs/rGO_NaBH$_4$ and 20% Pt/C electrodes.

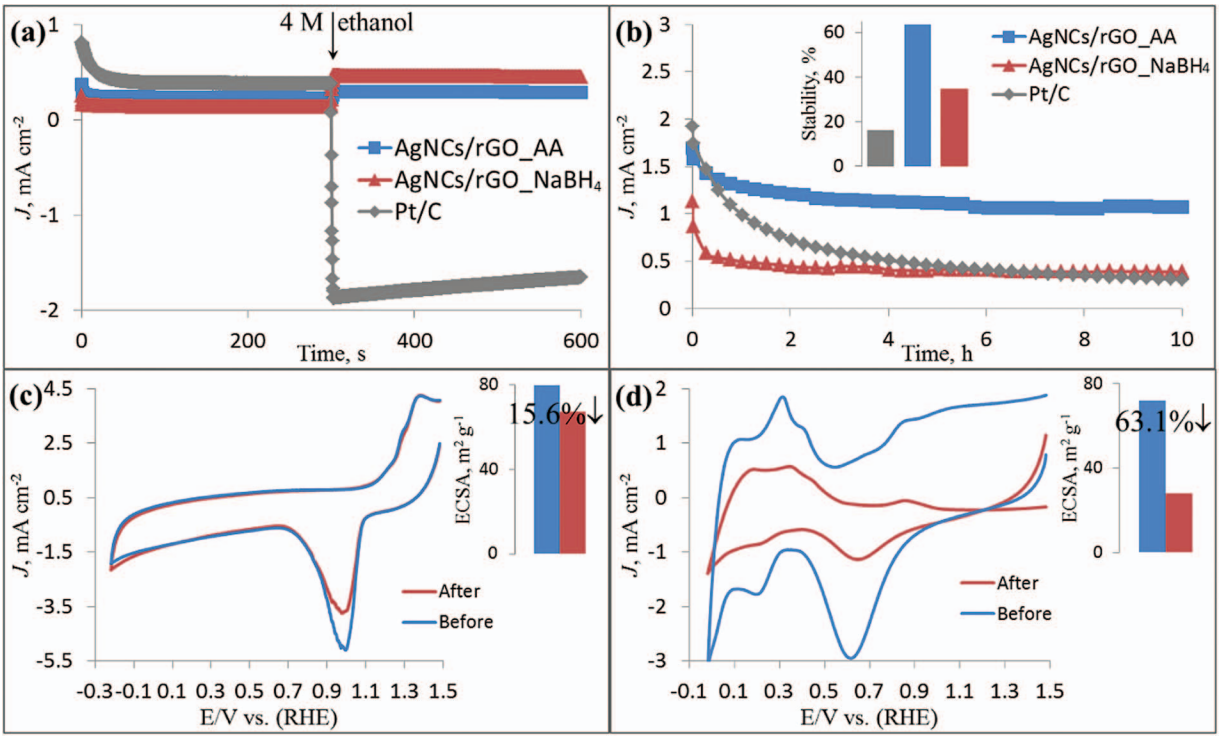

Figure 7. Amperometric responses obtained on AgNCs/rGO_AA, AgNCs/rGO_$NaBH_4$ and Pt/C electrodes for fuel selectivity test (with 4 M ethanol addition) (a) and stability test for 10 h (b) at an applied potential of 0.68 V (vs. RHE) at 1600 rpm rotation speed in O_2-saturated 0.1 M KOH; CV curves on AgNCs/rGO_AA (c) and Pt/C (d) catalysts in Ar-saturated 0.1 M KOH solution at a scan rate of 50 mV s^{-1} before and after 1,000 cycles; insets: stability as % (b) and ECSA comparison before and after stability test (c and d).

was same (~0.12 mA cm^{-2}) at 0.7 V for both catalysts. Very particularly, the AgNCs/rGO_AA, produced MA of 0.38 mA g_{Ag}^{-1} (at 0.7 V) and 0.55 mA g_{Ag}^{-1} (at 0.0 V) which is 20% and 40% greater than the Pt/C catalyst, 0.316 mA g_{Pt}^{-1} (at 0.7 V) and 0.39 mA g_{Pt}^{-1} (at 0.0 V), respectively. This is consistent with the relatively high calculated J_k (from Equation 9) for ORR at the AgNCs/rGO_AA electrode with respect to the Pt/C and AgNCs/rGO_$NaBH_4$ catalysts (Figure 6e). In all above parameters, the AgNCs/rGO_$NaBH_4$ catalyst has less ORR activity which was treated by common reductant, $NaBH_4$. Better comparison can be displayed. The Tafel plots were derived to further investigate the kinetic properties for all tested catalysts in Figure 6f. Generally, two Tafel slopes are commonly derived in a Tafel plot such as, 120 mV dec^{-1} and 60 mV dec^{-1} at low and high overpotentials, respectively. The 120 mV dec^{-1} indicates the fast electron transfer at the rate determining step to the transport of O_2 at the electrocatalyst.[67,68] It is, however, for AgNCs/rGO_AA and Pt/C, the Tafel slopes are 118 and 121 mV dec^{-1}, respectively, at the high overpotentials which are very close to the theoretical value and obviously better than AgNCs/rGO_$NaBH_4$ (151 mV dec^{-1}). The Tafel analysis results indicate the better ORR catalysis behavior with not only improved ORR mechanism and faster electron transfer but also much better rate-determining step at AgNCs/rGO_AA catalyst.

The resistance and stability of catalysts.—Resistance to crossover effects and stability of the ORR catalyst materials are important considerations for their practical application in FCs as cathode catalysts. The current vs. time responses for ORR at all catalysts were obtained in O_2-saturated 0.1 M KOH solution (Figure 7). As a result of the addition of 4 M ethanol into the O_2-saturated solution (Figure 7a), a feeble and lowest signal change was observed in the ORR current density at the AgNCs/rGO_AA catalyst (only 2.8%) than the ORR current for the Pt/C catalyst (100%), AgNCs/rGO_$NaBH_4$ (14.6%). Indicating AgNCs/rGO_AA has higher ORR selectivity and a good ability for avoiding crossover effects from alcohol-like fuels. Also, Figure 7b shows that the current density from all catalysts rapidly decreased initially and subsequently decreased slowly and reached a pseudo-steady state with increasing time. After 10 h continuous amperometric response under such condition, the AgNCs/rGO_AA (63.5%) exhibited a higher stability [final current density/initial current density, J_f/J_i*100] than the Pt/C (16.2%) and other tested catalysts (Figure 7b inset) which indicating the AgNCs/rGO_AA electrocatalyst is much more stable for long time use in DAFCs. We also performed accelerated durability tests by applying linear potential sweeps at 50 mV s^{-1} in Ar-saturated 0.1 M KOH solution. After 1,000 cycles, the CV measurements showed a loss of 15.6% in ECSA for the AgNCs/rGO_AA, and 63.1% for the Pt/C catalyst (Figures 7c and 7d), suggesting that the AgNCs/rGO_AA had better durability than the Pt/C catalyst.

Conclusions

The ORR catalysts based on AgNCs grafted onto rGO have synthesized through a simple chemical reduction process treating with AA reducing agents. The AA treated AgNCs/rGO, which greatly enhances $4e^-$ involved ORR electrocatalytic activity with lowering H_2O_2 formation than that of even commercially available 20 wt% Pt/C and conventional $NaBH_4$ treated catalysts. In instrumental characterization, AgNCs/rGO_AA shows not only a high crystalline structure, well dispersion and higher population of AgNCs but also higher degree of oxygenated groups removal from the edge with higher sp^2 conjugated network restoration of rGO, which are the key factor for faster electron transferred ORR in DAFCs. All experimental and kinetic results demonstrate that the AgNCs/rGO_AA catalyst could be employed as a potentially efficient, corrosive tolerance, highly stable and inexpensive ORR catalyst to replace Pt-based catalysts.

Acknowledgment

This work was supported in part by the National Research Foundation of Korea (15H1C1A1035825 and 15R1A4A1041746) and in part by Korea Electric Power Cooperation (KEPCO).

References

1. P. Gong, F. Du, Z. H. Xia, M. Durstock, and L. Dai, *Science*, **323**, 760 (2009).
2. M. S. Ahmed and S. Jeon, *J. Power Sources*, **218**, 168 (2012).
3. D. Kim, M. S. Ahmed, and S. Jeon, *J. Mater. Chem.*, **22**, 16353 (2012).
4. A. Shen, Y. Zou, Q. Wang, R. A. W. Dryfe, X. Huang, S. Dou, L. Dai, and S. Wang, *Angew. Chem.*, **126**, 10980 (2014).
5. M. S. Ahmed, D. Kim, and S. Jeon, *Electrochim. Acta*, **92**, 168 (2013).
6. M. Li, X. Bo, Y. Zhang, C. Han, A. Nsabimana, and L. Guo, *J. Mater. Chem. A*, **2**, 11672 (2014).
7. M. S. Ahmed and S. Jeon, *J. Electrochem. Soc.*, **161**, F1300 (2014).
8. B. Lim, M. J. P. Jiang, E. C. Cho, J. Tao, X. M. Lu, Y. M. Zhu, and Y. N. Xia, *Science*, **324**, 1302 (2009).
9. J. E. Choe, M. S. Ahmed, and S. Jeon, *J. Power Sources*, **281**, 211 (2015).
10. X. Zhou, Y. Gan, J. Du, D. Tian, R. Zhang, C. Yang, and Z. Dai, *J. Power Sources*, **232**, 310 (2013).
11. M. S. Ahmed and S. Jeon, *ACS Catal.*, **4**, 1830 (2014).
12. N.-S. Pai, P.-S. Chang, and S.-K. Yen, *Int. J. Hydrogen Energy*, **38**, 5259 (2013).
13. W. Chen, J. M. Kim, S. H. Sun, and S. W. Chen, *J. Phys. Chem. C*, **112**, 3891 (2008).
14. W. Chen and S. W. Chen, *Angew. Chem. Int. Ed.*, **48**, 4386 (2009).
15. Y. Y. Shao, J. Liu, Y. Wang, and Y. H. Lin, *J. Mater. Chem.*, **19**, 46 (2009).
16. X. Zhou, Z. Bai, M. Wu, J. Qiao, and Z. Chen, *J. Mater. Chem. A*, **3**, 3343 (2015).
17. K. Lee, M. S. Ahmed, and S. Jeon, *J. Power Sources*, **288**, 261 (2015).
18. M. S. Ahmed, H. S. Han, and S. Jeon, *Carbon*, **61**, 164 (2013).
19. S. Jin, M. Chen, H. Dong, B. He, H. Lu, L. Su, W. Dai, Q. Zhang, and X. Zhang, *J. Power Sources*, **274**, 1173 (2015).
20. L. Yuan, L. Jiang, J. Liu, Z. Xia, S. Wang, and G. Sun, *Electrochim. Acta*, **135**, 168 (2014).
21. S.-A. Park, H. Lim, and Y.-T. Kim, *ACS Catal.*, **5**, 3995 (2015).
22. K. Lee, M. S. Ahmed, and S. Jeon, *J. Electrochem. Soc.*, **162**, F1 (2015).
23. E. Jeong, M. S. Ahmed, H. Jeong, E. Lee, and S. Jeon, *Bull. Korean Chem. Soc.*, **32**, 800 (2011).
24. B. Wiley, Y. Sun, and Y. Xia, *Acc. Chem. Res.*, **40**, 1067 (2007).
25. L. Demarconnay, C. Coutanceau, and J.-M. Leger, *Electrochim. Acta*, **49**, 4513 (2004).
26. K. Okajima, K. Nabekura, T. Kondoh, and M. Sudoh, *J. Electrochem. Soc.*, **152**, D117 (2005).
27. J. C. Laura, K. Franklin, and J. Huang, *J. Am. Chem. Soc.*, **131**, 1043 (2009).
28. V. C. Tung, M. J. Allen, Y. Yang, and R. B. Kaner, *Nat. Nanotechnol.*, **4**, 25 (2009).
29. S. Wang, D. Yu, L. Dai, D. W. Chang, and J.-B. Baek, *ACS Nano*, **5**, 6202 (2011).
30. S. Stankovich, D. A. Dikin, R. D. Piner, K. A. Kohlhaas, A. Kleinhammes, Y. Jia, Y. Wu, S. T. Nguyen, and R. S. Ruof, *Carbon*, **45**, 1558 (2007).
31. K. S. Novoselov, A. K. Geim, S. V. Morozov, D. Jiang, Y. Zhang, S. V. Dubonos, I. V. Grigorieva, and A. A. Firsov, *Science*, **306**, 666 (2004).
32. H. Tanaka, S. Obata, and K. Saiki, *Carbon*, **59**, 472 (2013).
33. H. S. Han, M. S. Ahmed, H. Jeong, and S Jeon, *J. Electrochem. Soci.*, **162**, B75 (2015).
34. X. Wang, I. Kholmanov, H. Chou, and R. S. Ruoff, *ACS Nano*, **9**, 8737 (2015).
35. S. Yasmin, M. S. Ahmed,, D. Park, and S. Jeon, *J. Electrochem. Soci.*, **163**, B491 (2016).
36. H. Begum, M. S. Ahmed, and S. Jeon, *RSC Adv.*, **6**, 50572 (2016).
37. S. Stankovich, D. A. Dikin, G. H. B. Dommett, K. M. Kohlhaas, E. J. Zimney, E. A. Stach, R. D. Piner, S. T. Nguyen, and R. S. Ruoff, *Nature*, **442**, 282 (2006).
38. G. X. Wang, J. Yang, J. Park, X. L. Gou, B. Wang, H. Liu, and J. Yao, *J. Phys. Chem. C*, **112**, 8192 (2008).
39. M. S. Ahmed and S. Jeon, *J. Nanosci. Nanotechnol.*, **13**, 306 (2013).
40. S. Yasmin, M. S. Ahmed, and S. Jeon, *J. Electrochem. Soci.*, **162**, B363 (2015).
41. J.-M. You, M. S. Ahmed, H. S. Han, J. E. Choe, Z. Üstündag, and S. Jeon, *J. Power Sources*, **275**, 73 (2015).
42. D. Q. Yang, J. F. Rochette, and E. Sacher, *J Phys. Chem. B*, **109**, 4481 (2005).
43. X. Gao, J. Jang, and S. Nagase, *J. Phys. Chem. C*, **114**, 832 (2010).
44. D. W. Boukhvalov and M. I. Katsnelson, *J. Am. Chem. Soc.*, **130**, 10697 (2008).
45. K.-H. Wu, D.-W. Wang, and I. R. Gentle, *Carbon*, **73**, 234 (2014).
46. W. Yan, X. Cao, J. Tian, C. Jin, K. Ke, and R. Yang, *Carbon*, **99**, 195 (2016).
47. M. Favaro, L. Ferrighi, G. Fazio, L. Colazzo, C. D. Valentin, C. Durante, F. Sedona, A. Gennaro, S. Agnoli, and G. Granozzi, *ACS Catal.*, **5**, 129 (2015).
48. J. Zhang, H. Yang, G. Shen, P. Cheng, J. Zhang, and S. Guo, *Chem. Commun.*, **46**, 1112 (2010).
49. M. J. Fernandez-Merino, L. Guardia, J. I. Paredes, S. Villar-Rodil, P. Solís-Fernández, A. Martínez-Alonso, and J. M. D. Tascon, *J. Phys. Chem. C*, **114**, 6426 (2010).
50. M. van der Zande, R. J. Vandebriel, E. V. Doren, E. Kramer, Z. H. Rivera, C. S. Serrano-Rojero, E. R. Gremmer, J. Mast, R. J. B. Peters, P. C. H. Hollman, P. J. M. Hendriksen, H. J. P. Marvin, A. A. C. M. Peijnenburg, and H. Bouwmeester, *ACS Nano*, **6**, 7427 (2012).
51. D. C. Marcano, D. V. Kosynkin, J. M. Berlin, A. Sinitskii, Z. Sun, A. Slesarev, L. B. Alemany, W. Lu, and J. M. Tour, *ACS Nano*, **4**, 4806 (2010).
52. K. Cheng, Z. Kou, J. Zhang, M. Jiang, H. Wu, L. Hu, X. Yang, M. Pan, and S. Mu, *J. Mater. Chem. A*, **3**, 14007 (2015).
53. M. S. Ahmed, H. Jeong, J.-M. You, and S. Jeon, *Electrochim. Acta*, **56**, 4924 (2011).
54. Z. Zhang, C. Shao, Y. Sun, J. Mu, M. Zhang, P. Zhang, Z. Guo, P. Liang, C. Wang, and Y. Liu, *J. Mater. Chem.*, **22**, 1387 (2012).
55. T. Ghosh, B. Satpati, and D. Senapati, *J. Mater. Chem. C*, **2**, 2439 (2014).
56. M. S. Ahmed, D. Park, and S. Jeon, *J. Power Sources*, **308**, 180 (2016).
57. W.-P Xu, L.-C. Zhang, J.-P. Li, Y. Lu, H.-H. Li, Y.-N. Ma, W.-D. Wang, and S.-H. Yu, *J. Mater. Chem.*, **21**, 4593 (2011).
58. V. Grover, R. Shukla, R. Kumari, B. P. Mandal, P. K. Kulriya, S. K. Srivastava, S. Ghosh, A. K. Tyagi, and D. K. Avasthi, *Phys. Chem. Chem. Phys.*, **16**, 27065 (2014).
59. M. S. Ahmed and S. Jeon, *J. Power Sources*, **282**, 479 (2015).
60. C.-Y. Su, Y. Xu, W. Zhang, J. Zhao, X. Tang, C.-H. Tsai, and L.-J. Li, *Chem. Mater.*, **21**, 5674 (2009).
61. J. Liu, W. Lv, W. Wei, C. Zhang, Z. Li, B. Li, F. Kang, and Q.-H. Yang, *J. Mater. Chem. A*, **2**, 3031 (2014).
62. Z. Yang, Z. Yao, G. Li, G. Fang, H. Nie, Z. Liu, X. Zhou, X. Chen, and S. Huang, *ACS Nano*, **6**, 205 (2012).
63. X. Hu, Q. Zhu, X. Wang, N. Kawazoe, and Y. Yang, *J. Mater. Chem. A*, **3**, 17858 (2015).
64. W. Bian, Z. Yang, P. Strasser, and R. Yang, *J. Power Sources*, **250**, 196 (2014).
65. M. Yun, M. S. Ahmed, and S. Jeon, *J. Power Sources*, **293**, 380 (2015).
66. S. Du, Y. Lu, S. K. Malladi, Q. Xu, and R. Steinberger-Wilckens, *J. Mater. Chem. A*, **2**, 692 (2014).
67. S. J. Amirfakhri, D. Binny, J.-L. Meunier, and D. Berk, *J. Power Sources*, **257**, 356 (2014).
68. M. S. Ahmed, D. Kim, H. S. Han, H. Jeong, and S. Jeon, *J. Nanosci. Nanotechnol.*, **12**, 8349 (2012).